

<https://doi.org/10.1038/s43247-024-01592-4>

Latent magmatism beneath the Korean Peninsula caused by asthenosphere upwelling

Check for updates

Heejun Kim ^{1,2}, Hyunwoo Lee ¹✉, Jung-Hun Song ¹, Wonhee Lee ¹, Jungpyo Hong ^{1,3},
Takanori Kagoshima ^{4,5}, Naoto Takahata ⁴, Yuji Sano^{4,6} & Tobias P. Fischer ⁷

Volatiles such as helium and carbon dioxide provide insights into geological processes spanning from the Earth's deep interior to its surface. Integration with geophysical data providing enhanced vertical resolution with a wider horizontal range better elucidates the mantle dynamics and its interactions with the crust. Here we present geochemistry of volatiles dissolved in fluid samples from fault-related springs, thermal spa waters, and groundwaters across the Korean Peninsula. These were examined in conjunction with existing geophysical information. Remarkably, there is a strong spatial correlation between helium isotopes and S-wave velocity, suggesting the influence of mantle upwelling on both geochemical and geophysical parameters. Furthermore, the computed helium flux is comparable to that of volcanic regions, implying partial melting induced by mantle upwelling due to edge-driven convection beneath the Korean Peninsula. Therefore, these findings suggest that mantle-derived volatiles can be released diffusely over large areas through faults in the modern Earth's intraplate environment.

Volatiles are known to be effective tools for directly observing the influence of the mantle on the Earth's surface. As the asthenospheric mantle ascends and reaches the lithosphere, volatiles can be transported through volcanism or fault processes^{1–4}. Through interaction with fluids containing mantle-derived volatiles, the lithosphere in intra-plate settings, such as incipient continental rift zones, undergoes thinning with physical and thermal weakening, eventually resulting in the development of new divergent boundaries^{5,6}. Among volatiles, He that is the lightest noble gas and CO₂ that is the second most abundant component of volcanic gas after water vapor⁷ are widely used to trace mantle-derived components in plate margins (e.g., Sano and Marty⁸; Tardani et al.⁹). In particular, He isotopes are typically expressed as ³He/⁴He (1 Ra = 1.38 × 10^{−6}, refs. 10,11), and this ratio allows for a clear distinction between mantle and crustal values, effectively discerning the mantle signals from rock or fluid samples. Sources of CO₂ can be traced via carbon isotope compositions (δ¹³C), which can differentiate between the depleted upper mantle and recycled carbonate or organic matter-bearing slab materials (e.g., Tardani et al.⁹ and Lee et al.¹²).

While magmatism is predominant at plate boundaries, it also appears in the interiors of tectonic plates^{13–15}. The intra-plate magmatism is

associated with the break-up of the supercontinent, involving large igneous provinces (LIPs)¹⁶, which can trigger the development of continental rifts through the thermal weakening of the lithosphere¹⁷. In this context, it has been reported that in various modern continental rifting areas (e.g., East Africa and Rio Grande), the ³He/⁴He ratios and δ¹³C-CO₂ values of the asthenospheric mantle origin predominate in fault-related springs from regions with relatively thinner lithosphere, as a result of weakened physical properties of the plates due to magmatism by asthenospheric mantle upwelling^{3,12,18}.

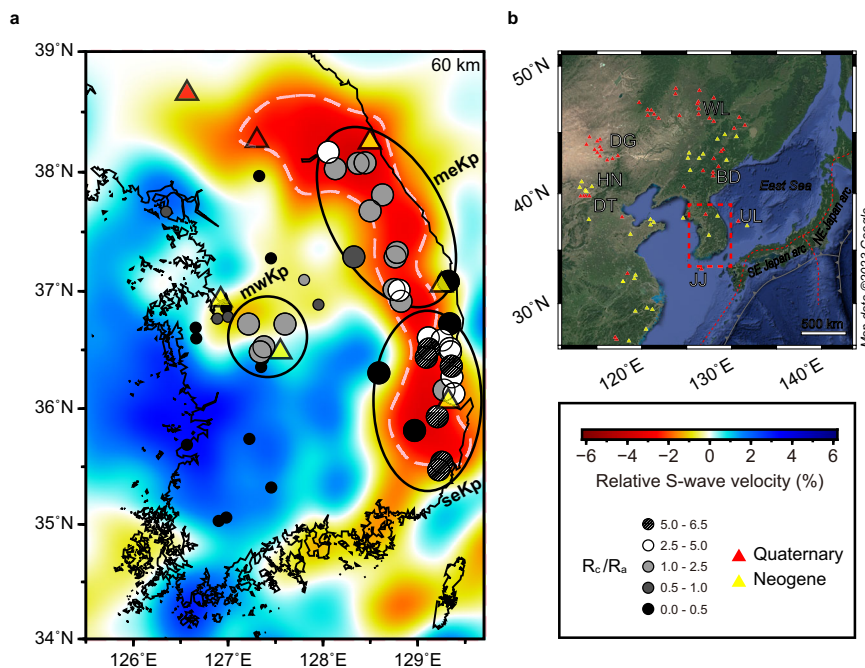
Northeast (NE) Asia, including the Korean Peninsula and China, became an intra-plate environment following the separation of the Japanese arc from the Eurasian plate during the East Sea back-arc opening^{19,20}. The late Cenozoic magmatism in this region has led to the emplacement of alkaline rocks across NE Asia (Fig. 1). ³He/⁴He ratios measured in olivine and clinopyroxene contained in these Cenozoic volcanic rocks range from 4.5 to 7.3 Ra, indicating potential mantle melting by lithosphere-asthenosphere interaction^{20,21}. Moreover, ³He/⁴He ratios in the mantle value range (up to 6.0 Ra) have been observed in groundwater and fault-related spring samples within the southeastern Korean Peninsula^{22–24}. Interestingly, seismic

¹School of Earth and Environmental Sciences, Seoul National University, Seoul, Republic of Korea. ²Ocean Georesources Research Department, Korea Institute of Ocean Science and Technology, Busan, Republic of Korea. ³Department of Earth and Environmental Sciences, University of Michigan, Ann Arbor, MI, USA.

⁴Atmosphere and Ocean Research Institute, University of Tokyo, Kashiwa, Japan. ⁵Graduate School of Science and Engineering, University of Toyama, Toyama, Japan. ⁶Center for Advanced Marine Core Research, Kochi University, Nankoku, Japan. ⁷Department of Earth and Planetary Sciences, University of New Mexico, Albuquerque, NM, USA. ✉e-mail: lhw615@snu.ac.kr

Fig. 1 | Helium isotope distribution on S-wave mantle tomography in the study area.

a Distribution of corrected He isotope compositions (R_c/R_a) of the samples (gray scale circles) and the distribution of the Korean Cenozoic volcanic rocks (yellow and red triangles) overlaid on the relative S-wave velocity map that represents S-wave perturbations at a depth of 60 km. Sampling locations are elliptically represented in three regions: mwKp (midwestern Korean peninsula), meKp (mideastern Korean peninsula), and seKp (southeastern Korean Peninsula). The larger circles are R_c/R_a ratios reported in this study, and the smaller circles are reference data^{63–66}. The region with velocity reductions exceeding -2% is delineated by dashed white lines. Most of the sampling locations are related to faults, and their distribution is shown in Supplementary Information. **b** The study area is boxed with red dashed lines in the NE Asia map, and the names of the Cenozoic volcanic areas in NE Asia are abbreviated as follows: Wudalianchi (WL), Dariganga (DG), Hannuoba (HN), Mt. Baekdu (BD), Datong (DT), Ulleung (UL), and Jeju (JJ). The satellite image is from Google Maps (2023) *North-east Asia, 22,500,000:1*, <https://goo.gl/maps/qC7f5ojgNtMLUdom9> [September 11, 2023].



tomography has detected distinctive slow velocities in the upper mantle mainly beneath the central and eastern coastal margins of the Korean Peninsula, indicative of asthenospheric upwelling accompanied with partial melting²⁵. Additionally, edge-driven convection (EDC) has been proposed as a possible mechanism for low velocity zone (LVZ) generation in the Northeast Asia region from evidence such as the heterogeneous distribution of LVZs controlled by the lithospheric thickness and the swelling that forms the mountain ranges present on the surface^{25,26}. However, a geochemical interpretation to support the presence of partial melting has not yet been attempted.

This study presents the comprehensive analytical results that combine geochemical and geophysical data from the Korean Peninsula, employing the following approaches. First, we assume that the fault-related springs distributed across South Korea are emitters of volatiles on the surface to test the existence of mantle upwelling. This assessment further confirms that the Korean Peninsula regions share a common mechanism with other continental areas that include intra-plate volcanism. Then, by integrating the measured He data with S-wave velocity tomography, we propose a potential magma distribution at the upper mantle level beneath the Korean Peninsula, addressing that mantle upwelling acts as a source of volatiles from the Cenozoic volcanic rocks and fluids in this region.

Results and discussion

Sources of volatiles

Based on the distribution of He isotope ratios, we found distinct areas with high $^3\text{He}/^4\text{He}$ ratios in the Korean Peninsula and divided it into three areas (Fig. 1 and Supplementary Information): the southeastern Korean Peninsula (seKp), the mideastern Korean Peninsula (meKp), and the midwestern Korean Peninsula (mwKp). In general, CO_2 and N_2 are the main components that make up 81 to 100 vol.% of the gases emitted from the fault-related springs (Supplementary Information). Among them, 18 samples have N_2 concentrations greater than 10 vol.%, and 10 out of them have N_2 concentrations greater than 75 vol.%. 22 samples show CO_2 concentrations higher than 90 vol.%. The range of He concentration is similar between mwKp (0.03 to 676.0 ppm) and seKp (0.07 to 613.5 ppm), but a slightly narrower range between 0.02 and 163.5 ppm is observed in meKp. The average concentrations of N_2 , O_2 , Ar, and CO_2 are similar between meKp (23.2%, 2.9%, 0.5%, and 74.2%, respectively), mwKp (15.5%, 2.9%, 0.2%,

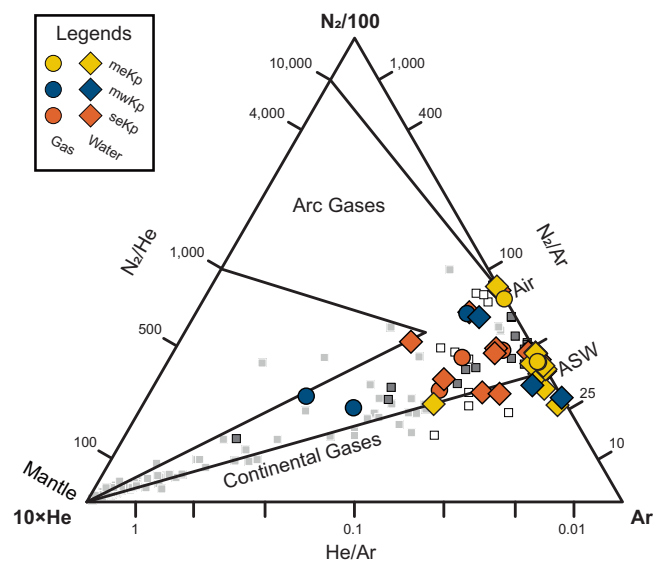


Fig. 2 | N_2 -He-Ar ternary plot. MORB and ASW refer to Mid-Ocean Ridge Basalts and Air-Saturated Water, respectively. Reference values are from Gyeonju, Ulsan, and Busan in South Korea²² (white squares), Pohang in South Korea²³ (dark gray squares), and global continental rift gases¹² (light gray squares). All of the following figures use the same symbols.

and 82.8% respectively), and seKp (36.0%, 1.7%, 0.6%, and 61.9%, respectively), with CH_4 up to 0.6% in some samples of seKp. Our samples show a mixing relationship between atmospheric (Air-ASW) and endogenic (mantle-crustal) components based on the N_2 -Ar-He ternary diagram (Fig. 2), which is consistent with previous studies in the SE Korean Peninsula^{22,23}. In addition, the subduction zone signatures (e.g., elevated N_2/He and N_2/Ar ratios in Fig. 2) were not identified in the study area as previously reported^{22,23}.

The sources of He are investigated by using $^3\text{He}/^4\text{He}$ ratios and reciprocal $^4\text{He}/^{20}\text{Ne}$ ratios (Fig. 3). Overall, $^3\text{He}/^4\text{He}$ ratios of the fluid samples in the Korean Peninsula range from a maximum of 6.2 Ra to a minimum of

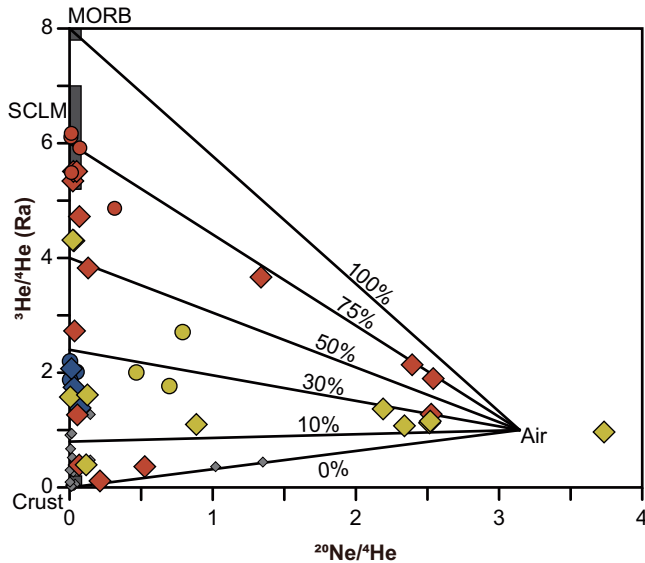


Fig. 3 | $^3\text{He}/^4\text{He}$ (R/Ra) vs. $^{20}\text{Ne}/^4\text{He}$ plot. Mixing lines between each end-member (MORB, SCLM, crust, and air) are shown with a percentage contribution from the MORB mantle source. Reference values are shown as gray diamonds^{63–66}.

0.1 Ra, and $^4\text{He}/^{20}\text{Ne}$ ratios range from 0.3 to 342.8, with an average of 45.6. As 30 samples out of 39 samples have higher $^4\text{He}/^{20}\text{Ne}$ ratios than 1, the effect of air contamination on He isotopes is unlikely to be severe. Since LVZs are located in the deeper levels than the lithospheric thickness²⁷, we selected the asthenospheric mantle as the original source of volatiles rather than sub-continental lithospheric mantle (SCLM). It seems that He emitted from the asthenospheric mantle beneath the Korean Peninsula is affected by various degrees of the contributions from the SCLM (6.1 ± 0.9 Ra, ref. 28) and continental crust (0.02 Ra, ref. 29) end-members. The highest $^3\text{He}/^4\text{He}$ ratio in each region is seKp (6.2 Ra), meKp (4.3 Ra), and mwKp (2.2 Ra) indicating that springs with an obvious mantle contribution are spatially well distributed, especially in the seKp area (Fig. 1).

The $\delta^{13}\text{C}\text{-CO}_2$ values of the samples (vs. Vienna Pee Dee Belemnite) range from -20.2 to -3.7 ‰. When the $\text{CO}_2/{}^3\text{He}$ ratio is considered together, two main trends appear (Fig. 4). First, it has a range similar to the $\delta^{13}\text{C}\text{-CO}_2$ of the mid-ocean ridge basalts (MORB) mantle (-6.5 ± 2.5 ‰, ref. 8), but shows a wide range of $\text{CO}_2/{}^3\text{He}$ ratios (up to 2.81×10^{13}). This vertical trend suggests 1) crustal contamination or 2) the effect of degassing fractionation on gas components associated with the difference in solubility of CO_2 and He in hydrothermal systems without considerable impact on isotopic change^{9,11}. Another geochemical feature in our CO_2 data is the tendency of $\text{CO}_2/{}^3\text{He}$ ratios to decrease with $\delta^{13}\text{C}\text{-CO}_2$ values. Although the $\delta^{13}\text{C}\text{-CO}_2$ values of some of these samples alone can indicate organic CO_2 , previous studies of gas and rock samples around the Korean Peninsula suggested that slab-derived volatiles are not detectable^{20–24}, which is also not observed in the $\text{N}_2\text{-Ar-He}$ systematics (Fig. 2). Instead, it is more likely that CO_2 removal occurred due to precipitation of carbonate controlled by pH in water^{30–32}. In support of this, the linear relationship between CO_2 concentration and pH (Supplementary Information) exhibits a fairly valid correlation ($R^2 = 0.52$), implying that CO_2 loss may have occurred in some high pH springs in the Korean Peninsula, as previously reported in seKp²³. Therefore, we propose that CO_2 emitted through the fault-related springs of the Korean Peninsula is originally from the mantle, assuming that there were no effects of degassing fractionation and CO_2 loss.

The origins of N_2 , another major gas component, were traced by $\delta^{15}\text{N}\text{-N}_2$ (-8.0 to 3.3 ‰ vs. Air) values and $\text{N}_2/{}^3\text{He}$ ratios (Fig. 5). If we used the conventional $\delta^{15}\text{N}\text{-N}_2/{}^3\text{He}$ mixing diagram of the MORB mantle (-5 ‰; 8.9×10^5), air (0 ‰; 1.0×10^{11}), and sediment (7 ‰; 1.4×10^{12}) end-members³³, some data points from the meKp and seKp samples are out of

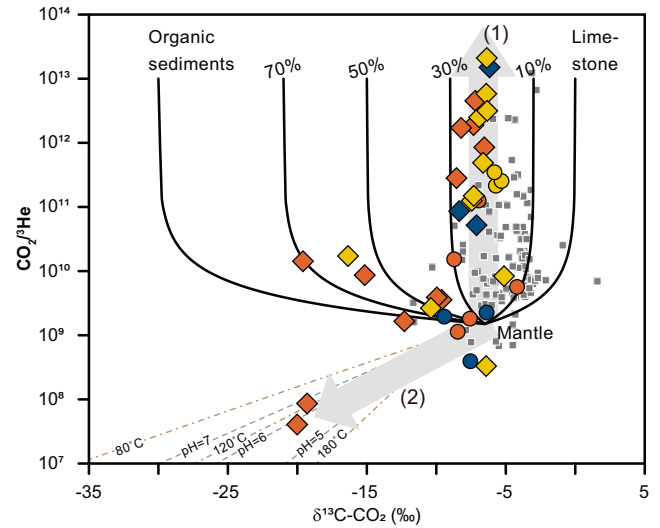


Fig. 4 | $\text{CO}_2/{}^3\text{He}$ vs. $\delta^{13}\text{C}\text{-CO}_2$ plot. The percentage of organic sediment contributions of the crustal end-members are displayed. Global continental rift gases are shown¹² (open gray boxes). Trend (1) indicates degassing fractionation and trend (2) reflects the effects of calcite precipitation (brown dashed lines) at various temperatures and water-gas interaction (gray dashed lines) under various pH conditions at 15 °C.

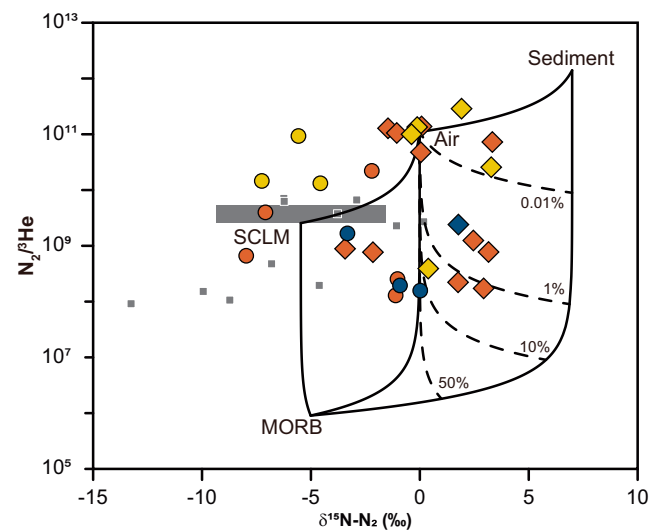


Fig. 5 | $\text{N}_2/{}^3\text{He}$ vs. $\delta^{15}\text{N}\text{-N}_2$ plot. The SCLM range (1σ area around the average value) is from xenoliths (noted by gray squares) in Sveyagin, Far East Russia³⁶. The solid lines connect each end-member (MORB, SCLM, sediment, and air). The dashed lines display the contribution of mantle to sediment for quantitative tracing of nitrogen sources, and the larger the air end-member contributes, the closer they are to the mantle-air mixing line.

mixing relationship. Unlike the increase in $\text{CO}_2/{}^3\text{He}$ ratios due to degassing fractionation shown in the mixing diagram of CO_2 (Fig. 4), for $\text{N}_2/{}^3\text{He}$, N_2 is 72 times and He is 200 times less soluble in Henry's law compared to CO_2 in the low temperature water (0 °C) (refs. 34,35). Thus, as both N_2 and He have very low solubility in similar orders, it is likely that the degassing fractionation effect is insignificant for the $\text{N}_2/{}^3\text{He}$ ratios of the samples. To address this off-trend samples in three component mixing, we show the local SCLM-derived N_2 source from the reported $\delta^{15}\text{N}\text{-N}_2$ range of mantle xenoliths in Far Eastern Russia³⁶. Since the $\delta^{15}\text{N}\text{-N}_2$ heterogeneity in the lithospheric mantle has been suggested regionally (e.g., Fischer et al.³⁷), we attempted to account for the cause of some of the deviation values has been resolved by applying the local

end-member. As chemical composition of the SCLM beneath the Korean Peninsula is not reported yet, spatially closest data of the SCLM (i.e. Far East Russia) would be the most plausible substitution. This could indicate that the SCLM interacting with the ascending asthenospheric mantle with partial melts, underwent metasomatism and became the potential N₂ source. Although some data points show sediment contributions, the air contribution seems to be more striking. Regarding the formation of Cenozoic magmas in NE Asia, the involvement of the SCLM has been proposed to have driven by lithosphere-asthenosphere interaction^{20,21}. In the same context, as the lowest δ¹⁵N (< 0‰) decreases when S-wave velocity decreases (Supplementary Information), implying that endogenic N₂ from the SCLM or the asthenospheric mantle tends to be emitted from LVZs.

Distribution of He isotope ratios related to mantle upwelling

In NE Asia, lithosphere and asthenosphere boundary (LAB) depths typically range from 50 km to 250 km, and the Cenozoic volcanoes are mainly distributed in areas with LAB depths less than 75 km (ref. 38). Referring to this, we examined the spatial distribution of seismic velocity anomalies at a depth of 60 km (Fig. 1a) and the averaged S-wave anomaly at depths from 40 to 100 km (Supplementary Information), which are in range of the lithospheric thickness in the Korean Peninsula and NE China²⁷. In the 40 to 100 km depth range, the values at each depth and the average for the interval show similarity to each other (Supplementary Information), but the horizontal contrast of the physical properties at a depth of 60 km can be most clearly shown with respect to the resolution of the mantle tomography model. Considering this, the tomographic image with a depth of 60 km was selected as the representative (Figs. 1a and 6). To quantitatively visualize the correlation between mantle-derived helium and LVZs, we plotted R_c/R_a ratios and relative S-wave velocity values together (Fig. 6). The enveloping line between the maximum values of the R_c/R_a ratios and the relative S-wave velocity indicates a negative correlation. A majority of samples with lower ³He/⁴He ratios (e.g., R_c/R_a < 1) are distributed from slightly negative (> -1%) to positive S-wave anomalies, which is attributed to the influence of Precambrian metamorphic rocks and Mesozoic granitoids with abundant U and Th³⁹. Lee et al.²² reported the results of R_c/R_a < 0.1 related to the distribution of granitoids in the seKp area. However, the elevated R_c/R_a

ratios (e.g., > 1 Ra) and other mantle-derived volatiles (e.g., CO₂ and N₂) are displayed only within areas with negative S-wave anomalies, implying an obvious mantle contribution.

Implications for potential magmatism

In the crustal and mantle ⁴He flux plot (Fig. 7), samples from volcanic region and tectonic strain processes can be clearly distinguished⁴⁰. In addition, magmatism is thought to have higher crustal ⁴He fluxes as well as mantle ⁴He fluxes compared to the values related to the tectonic strain degassing⁴¹. Using the above method, the ⁴He flux values of crust and mantle calculated from our samples (Supplementary Information) were plotted together with those of Okinawa Trough, Taiwan, Taupo, Yellowstone, and Magadi-Natron, where volcanic ⁴He flux values have previously been reported^{12,40-43}. Except for 4 samples with lower mantle ⁴He flux values, where thermal spa waters are highly affected by radiogenic ⁴He at the crustal level (Supplementary Information), most data points are plotted in the volcanic region (Fig. 7). In general, it has been suggested that mantle He could be emitted through faulting in non-volcanic areas (e.g., San Andreas Fault⁴). Likewise, it was proposed that mantle He is discharged through the active faults extending beyond the crustal thickness, considering no active volcanoes currently in the Korean Peninsula²²⁻²⁴. However, our calculated ⁴He fluxes refute the aforementioned model and can support that regions with negative S-wave anomalies are consistent with the distribution of Neogene and Quaternary volcanic rocks (Fig. 1b). Specifically, the Quaternary volcanic rocks in Ulleung and Jeju (Fig. 1b), which were suggested to be produced as a consequence of lithosphere-asthenosphere interaction, show similar R/R_a ratios (3.5 to 7.3 Ra) to our samples^{20,21}. Furthermore, the Cenozoic volcanic rocks (< 0.1 to 30 Ma) in the central North China Craton region adjacent to the Korean Peninsula have been addressed to originate from deep magma sources distributed at the LAB (90 and 130 km, ref. 44). In the North China Craton area, R_c/R_a ratios have been reported up to 2.08 in hot springs and geothermic wells with negative V_p anomaly mainly observed at a depth of 70 km, indicating that the mantle-derived volatiles are emitted from faults through asthenospheric mantle upwelling⁴⁵.

Comprehensively, our results address the occurrence of partial melting or the existence of deep magma beneath the Korean Peninsula. By illustrating the He degassing characteristics of the Korean Peninsula

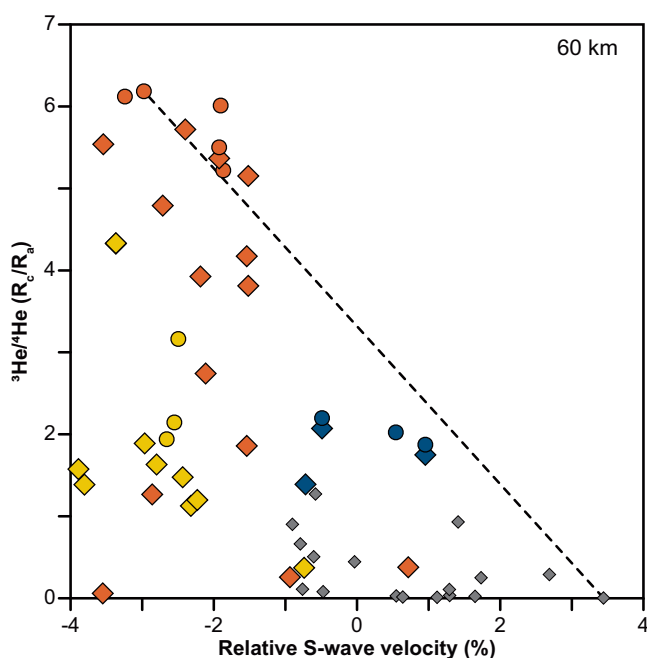


Fig. 6 | ³He/⁴He ratios vs. relative S-wave velocity (at a depth of 60 km) plot. The dashed line represents the negative correlation of the maximum values between the R_c/R_a ratios and the relative S-wave velocities. Reference values are noted by gray diamonds⁶³⁻⁶⁶.

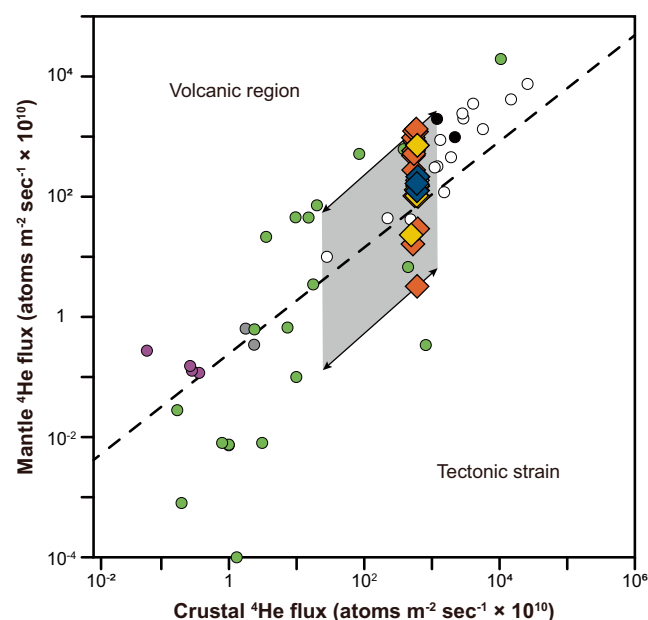


Fig. 7 | Crustal and mantle ⁴He flux plot. Flux values of the samples were calculated with a porosity value (Φ) of 0.01, and the gray area is a computed range for the samples with different porosity values from 0.005 to 0.2. Reference values are from Okinawa Trough⁴² (purple), Taiwan⁴³ (gray), Yellowstone⁴¹ (black), Magadi-Natron¹² (white with black outline), and other areas⁴⁰ (green).

(Fig. 1), we propose potential magmatism beneath the Korean Peninsula based on the following rationales; 1) the primary source of volatiles is inferred to be the mantle; 2) the presence of asthenospheric mantle signals at shallow upper mantle depths is evidenced by the negative S-wave anomaly, elevated Rc/Ra ratios, and the spatial distribution of Cenozoic volcanic rocks across the Korean Peninsula; and 3) the ^4He flux values of the mantle and the crust show a volcanic region trend. Our findings propose that Cenozoic intraplate magmatism in NE Asia may not be limited to the distributed volcanic rocks but could exist more extensively as latent magmatism, which emits mantle-derived volatiles that can be observed on the Earth's surface.

To explain N-S elongated cratonic root and low velocity zone, we suggest that EDC is the LVZ generation mechanism^{25,26}. The eastern part of the Korean Peninsula underwent thinning during the East sea (Sea of Japan, Fig. 1a) back-arc opening. This thinning event generated a heterogeneous lithospheric thickness difference between thicker western cratonic and thinner eastern regions, inducing decompression melting perpendicular to the lithosphere thickness gradient²⁷. Taking this into account, we hypothesized that EDC may occur in slow plate movement environments (< 1 cm/yr, Kaislaniemi and van Hunen⁴⁶), such as the Korean Peninsula⁴⁷. As a result, partial melting occurring in the asthenospheric mantle from this process supports that the volatiles have geochemical properties similar to those of gases emitted from other continental rifts. Since the stagnant Pacific slab physically separates the lower mantle and upper mantle layers in the mantle transition zone (410–660 km depth)^{48,49}, it is difficult for any large-scale lower mantle plume to affect the Korean Peninsula. Additionally, the seismic velocity anomaly is concentrated in the upper mantle (50 to 120 km depth) than deeper regions (~ 300 km, ref. 25). Furthermore, as the opening of the East Sea (Sea of Japan) progressed, the source of volcanic rocks was mainly contributed by metasomatized SCLM from arc magma, and as the plate thinning continued, the asthenosphere component eventually prevailed without the lower mantle plume components^{50,51}. Finally, the geochemical characteristics of volatiles, including helium derived from the upper mantle emitted from the Korean Peninsula, are particularly affected by the lithospheric thickness, indicating that EDC is a major mechanism for the Cenozoic magmatism in Northeast Asia. Furthermore, it suggests that larger-scale mantle degassing may occur globally and that the total flux of volatiles may be underestimated.

Methods

Sampling and gas analysis

30 samples (18 water samples, 3 thermal spa water samples, and 9 gas samples) from 26 sampling sites (Fig. 1; Supplementary Information) were measured to obtain gas composition, and isotope ratios of $^3\text{He}/^4\text{He}$, $\delta^{13}\text{C}-\text{CO}_2$, $\delta^{15}\text{N}-\text{N}_2$, and $^{36}\text{Ar}/^{40}\text{Ar}$. Additionally, 9 previously reported samples from the SE Korean Peninsula were discussed together^{22–24}. Both bubbling and dissolved gases in water samples analyzed at the Atmosphere and Ocean Research Institute (AORI), the University of Tokyo (e.g., Lee et al.²² and Kim et al.²³). For water samples, dissolved gases were extracted in the high vacuum system before analysis. Concentrations (CO_2 , N_2 , O_2 , CH_4 , Ar, and He) of gases were measured by a Pfeiffer Prisma QMS 200 quadrupole mass spectrometer (QMS). $\delta^{13}\text{C}$ of CO_2 and $\delta^{15}\text{N}$ of N_2 were measured by an isotope ratio mass spectrometer (Isoprime 100 by Elementar). To determine $^3\text{He}/^4\text{He}$ and $^4\text{He}/^{20}\text{Ne}$ ratios, dissolved gas samples were purified by titanium getters at 400 °C and charcoal traps at liquid nitrogen temperature (77 K). After measuring $^4\text{He}/^{20}\text{Ne}$ ratios via online QMS (Prisma QMS 200 by Pfeiffer), Neon was trapped by the cryogenic pump at 40 K. Then, purified He was injected into a noble gas mass spectrometer (Helix SFT by ThermoFisher) to measure $^3\text{He}/^4\text{He}$ ratios. He isotope ratios were calibrated using the internal He standard of Japan (HESJ, ref. 52), the air, and the air saturated water (ASW). In another vacuum line, argon was purified using a liquid nitrogen temperature U-trap and titanium getter at 600 °C, and analyzed by QMS (MKS Microvision-2). Measured $^3\text{He}/^4\text{He}$ ratios (R/Ra) were corrected to eliminate the air-derived He effect for each sample. Postulating ^{20}Ne as an air-derived component⁵³, the pristine $^3\text{He}/^4\text{He}$ ratios of samples in the absence of

air contamination can be calculated as below⁵⁴:

$$R_c/R_a = [(^3\text{He}/^4\text{He})_{\text{measured}} - r]/(1 - r) \quad (1)$$

and

$$r = (^4\text{He}/^{20}\text{Ne})_{\text{ASW}} / (^4\text{He}/^{20}\text{Ne})_{\text{measured}} \quad (2)$$

where R_c/R_a is the corrected $^3\text{He}/^4\text{He}$ ratio in R/Ra notation, and $(^4\text{He}/^{20}\text{Ne})_{\text{ASW}}$ is the $^4\text{He}/^{20}\text{Ne}$ of ASW. In this study, we used the $^4\text{He}/^{20}\text{Ne}$ value of sample #8 as $(^4\text{He}/^{20}\text{Ne})_{\text{ASW}}$, where sample #8 shows a typical ASW signature (Supplementary Information).

S wave modelling and He flux estimation

We used a three-dimensional S-wave tomography model of the southern Korean Peninsula²⁵. We focus on seismic velocities at depths ranging from 40 to 100 km, which correspond to the upper mantle. The geophysical methods, datasets, and model resolutions can be found in Song et al.²⁵. Through the velocity model, volumetric local velocity heterogeneities in the crust and upper mantle have been estimated in greater detail. Crustal thicknesses were derived from Moho depth datasets around the southern Korean Peninsula obtained from receiver function analyses^{55–57}.

As mentioned in the previous sections, it was suggested that volatiles from mantle or crustal sources are transported mainly through permeable faults. Thus, the helium flux values emitted from the Korean Peninsula were calculated. First, the current ^4He production from the crust, $P(\text{He})$, can be computed as follows:

$$P(\text{He}) = \rho_c \times (1.19 \times 10^{-13} \times [\text{U}] + 2.88 \times 10^{-14} \times [\text{Th}]) \times (1 - \Phi) / \Phi \quad (3)$$

where Φ is the porosity of the fluid path, and $[\text{U}]$ and $[\text{Th}]$ are the U and Th concentrations of the crust, respectively. 1.19×10^{-13} and 2.88×10^{-14} are the ^4He production rates of U and Th, respectively (ref. 58). Using the computed $P(\text{He})$, the He flow rate ($q\text{He}$) can be acquired as below:

$$q\text{He} = \frac{H_c \rho_c P(\text{He})}{\rho_f [\text{He}]_{\text{F.m}}} \times \left[\frac{R_s - R_c}{R_m - R_s} \right] \quad (4)$$

where H_c is the crustal thickness; ρ_c and ρ_f are the density of the crust and the fluid (water, 1 g/cm^3); $[\text{He}]_{\text{F.m}}$ is the He concentration of the mantle-derived fluid; R_s , R_c , R_m are $^3\text{He}/^4\text{He}$ of the sample, the crust (0.02 Ra, ref. 29), and the MORB mantle (8 Ra, ref. 59), respectively. We used geophysical data for the crustal thickness as described above. For all samples, the average composition ($[\text{U}] = 1.3$ ppm and $[\text{Th}] = 5.6$ ppm) and the crustal density (2.8 g/cm^3) were substituted⁶⁰. $[\text{He}]_{\text{F.m}}$ was calculated from the sample He concentration and R_s , where postulating the $^3\text{He}/^4\text{He}$ ratio of sample helium is the simple mixture of 0.02 Ra of the crustal He (R_c) and 8 Ra of the mantle He (R_m). Using the acquired $q\text{He}$ and He concentration of each sample, the ^4He flux of each sample site was determined. All variables in Eqs. (3) and (4) except Φ were defined or measured. Therefore, the He flow rate and flux are functions of Φ . To further specify processes of how mantle He is released, we estimated distinction in ^4He fluxes between the mantle and crust contributions by using the conditions of 1) concentration of volatiles in water, 2) crustal thickness, 3) crustal porosity, and 4) Rc/Ra ratios^{1,40,61,62}. We postulated Φ (0.01) and its possible range (0.005 to 0.2) from previous studies^{1,40,62}. The He fluxes are from 1.13×10^2 to $1.48 \times 10^6 \text{ cm}^3/\text{yr}$ with $\Phi = 0.005$ and from 2.26×10^0 to $2.97 \times 10^4 \text{ cm}^3/\text{yr}$ with $\Phi = 0.2$. Total ^4He fluxes are from 1.12×10^3 to $4.16 \times 10^3 \text{ atoms/m}^2/\text{sec} \times 10^{10}$ with $\Phi = 0.005$ and from 2.25×10^1 to $8.37 \times 10^1 \text{ atoms/m}^2/\text{sec} \times 10^{10}$ with $\Phi = 0.2$ (Supplementary Information).

Data availability

The data supporting the findings of this study are included in Supplementary Information.

Received: 9 November 2023; Accepted: 31 July 2024;

Published online: 12 August 2024

References

- Kennedy, B. M. et al. Mantle fluids in the san andreas fault system, California. *Science* (80-) **278**, 1278–1281 (1997).
- Sano, Y., Nakamura, Y., Wakita, H., Urabe, A. & Tominaga, T. Helium-3 emission related to volcanic activity. *Science* (80-) **224**, 150–151 (1984).
- Karlstrom, K. E., Crossey, L. J., Hilton, D. R. & Barry, P. H. Mantle ^3He and CO_2 degassing in carbonic and geothermal springs of Colorado and implications for neotectonics of the Rocky Mountains. *Geology* **41**, 495–498 (2013).
- Klemperer, S. L. et al. Limited underthrusting of India below Tibet: $^3\text{He}/^4\text{He}$ analysis of thermal springs locates the mantle suture in continental collision. *Proc. Natl. Acad. Sci. USA* **119**, 1–7 (2022).
- Wang, H., van Hunen, J. & Pearson, D. G. The thinning of subcontinental lithosphere: the roles of plume impact and metasomatic weakening. *Geochem. Geophys. Geosyst.* **16**, 1156–1171 (2015).
- Muirhead, J. D. et al. Evolution of upper crustal faulting assisted by magmatic volatile release during early-stage continental rift development in the East African Rift. *Geosphere* **12**, 1670–1700 (2016).
- Fischer, T. P. & Chiodini, G. Volcanic, Magmatic and Hydrothermal Gases. in *The Encyclopedia of Volcanoes* 779–797 (Elsevier, 2015). <https://doi.org/10.1016/B978-0-12-385938-9.00045-6>.
- Sano, Y. & Marty, B. Origin of carbon in fumarolic gas from island arcs. *Chem. Geol.* **119**, 265–274 (1995).
- Tardani, D. et al. Exploring the structural controls on helium, nitrogen and carbon isotope signatures in hydrothermal fluids along an intra-arc fault system. *Geochim. Cosmochim. Acta* **184**, 193–211 (2016).
- Ozima, M. & Podosek, F. A. *Noble Gas Geochemistry*. (Cambridge University Press, 2002).
- Sano, Y., Marty, B. & Burnard, P. Noble Gases in the Atmosphere. in *The Noble Gases as Geochemical Tracers* (ed. Burnard, P.) 17–31 (Springer Berlin Heidelberg, 2013). https://doi.org/10.1007/978-3-642-28836-4_2.
- Lee, H. et al. Incipient rifting accompanied by the release of subcontinental lithospheric mantle volatiles in the Magadi and Natron basin, East Africa. *J. Volcanol. Geotherm. Res.* **346**, 118–133 (2017).
- Turcotte, D. L. & Oxburgh, E. R. Intra-plate volcanism. *Philos. Trans. R. Soc. London. Ser. A, Math. Phys. Sci.* **288**, 561–579 (1978).
- Conrad, C. P., Bianco, T. A., Smith, E. I. & Wessel, P. Patterns of intraplate volcanism controlled by asthenospheric shear. *Nat. Geosci.* **4**, 317–321 (2011).
- Pirajno, F., Ernst, R. E., Borisenko, A. S., Fedoseev, G. & Naumov, E. A. Intraplate magmatism in Central Asia and China and associated metallogeny. *Ore Geol. Rev.* **35**, 114–136 (2009).
- Ernst, R. E. *Large Igneous Provinces* **653** (Cambridge University Press, 2014).
- Brune, S. et al. Geodynamics of continental rift initiation and evolution. *Nat. Rev. Earth Environ.* **4**, 235–253 (2023).
- Muirhead, J. D. et al. Displaced cratonic mantle concentrates deep carbon during continental rifting. *Nature* **582**, 67–72 (2020).
- Cheon, Y. et al. Tectonically controlled multiple stages of deformation along the Yangsan Fault Zone, SE Korea, since Late Cretaceous. *J. Asian Earth Sci.* **170**, 188–207 (2019).
- Lee, W. et al. Trace element and helium isotope geochemistry of the Cenozoic intraplate volcanism in the East Sea (Sea of Japan): Implications for lithosphere–asthenosphere interaction. *Lithos* **388–389**, 106075 (2021).
- Kim, D. et al. Helium isotopes and olivine geochemistry of basalts and mantle xenoliths in Jeju Island, South Korea: Evaluation of role of SCLM on the Cenozoic intraplate volcanism in East Asia. *Lithos* **390–391**, 106123 (2021).
- Lee, H. et al. Mantle degassing along strike-slip faults in the Southeastern Korean Peninsula. *Sci. Rep.* **9**, 15334 (2019).
- Kim, H. et al. Mantle-Derived Helium Emission near the Pohang EGS Site, South Korea: Implications for Active Fault Distribution. *Geofluids* **2020**, (2020).
- Hong, J. et al. Fault-related basins as carbon reservoirs: Soil CO_2 emissions in the SE Korean Peninsula. *CATENA* **231**, 107300 (2023).
- Song, J.-H., Kim, S. & Rhie, J. Heterogeneous modification and reactivation of a craton margin beneath the Korean Peninsula from teleseismic travel time tomography. *Gondwana Res.* **81**, 475–489 (2020).
- Sun, Y. & Liu, M. Edge-driven asthenospheric convection beneath the North China Craton: A numerical study. *Tectonophysics* **849**, 229726 (2023).
- Lee, S., Saxena, A., Song, J. H., Rhie, J. & Choi, E. Contributions from lithospheric and upper-mantle heterogeneities to upper crustal seismicity in the Korean Peninsula. *Geophys. J. Int.* **229**, 1175–1192 (2022).
- Gautheron, C., Moreira, M. & Allègre, C. He, Ne and Ar composition of the European lithospheric mantle. *Chem. Geol.* **217**, 97–112 (2005).
- Andrews, J. N. The isotopic composition of radiogenic helium and its use to study groundwater movement in confined aquifers. *Chem. Geol.* **49**, 339–351 (1985).
- Zhang, J., Quay, P. D. & Wilbur, D. O. Carbon isotope fractionation during gas-water exchange and dissolution of CO_2 . *Geochim. Cosmochim. Acta* **59**, 107–114 (1995).
- Taran, Y., Morán-Zenteno, D., Inguaggiato, S., Varley, N. & Luna-González, L. Geochemistry of thermal springs and geodynamics of the convergent Mexican Pacific margin. *Chem. Geol.* **339**, 251–262 (2013).
- Suda, K. et al. Origin of methane in serpentinite-hosted hydrothermal systems: The $\text{CH}_4\text{-H}_2\text{-H}_2\text{O}$ hydrogen isotope systematics of the Hakuba Happo hot spring. *Earth Planet. Sci. Lett.* **386**, 112–125 (2014).
- Sano, Y., Takahata, N., Nishio, Y., Fischer, T. P. & Williams, S. N. Volcanic flux of nitrogen from the Earth. *Chem. Geol.* **171**, 263–271 (2001).
- Wilhelm, E., Battino, R. & Wilcock, R. J. Low-pressure solubility of gases in liquid water. *Chem. Rev.* **77**, 219–262 (1977).
- Sorey, M. L. et al. Carbon dioxide and helium emissions from a reservoir of magmatic gas beneath Mammoth Mountain, California. *J. Geophys. Res. Solid Earth* **103**, 15303–15323 (1998).
- Yamamoto, J. et al. Nitrogen and noble gas isotopic compositions of mantle xenoliths from Far Eastern Russia: Implications for nitrogen isotopic characteristics of mantle wedge fluid. *Earth Planet. Sci. Lett.* **534**, 116109 (2020).
- Fischer, T. P., Takahata, N., Sano, Y., Sumino, H. & Hilton, D. R. Nitrogen isotopes of the mantle: Insights from mineral separates. *Geophys. Res. Lett.* **32**, 1–5 (2005).
- Zhou, Z. et al. Undulating electrical lithosphere–asthenosphere boundary beneath Northeast China; as revealed by long-period magnetotelluric data. *Tectonophysics* **851**, (2023).
- Chough, S. K., Kwon, S. T., Ree, J. H. & Choi, D. K. Tectonic and sedimentary evolution of the Korean peninsula: A review and new view. *Earth Sci. Rev.* **52**, 175–235 (2000).
- Torgersen, T. Continental degassing flux of ^4He and its variability. *Geochem. Geophys. Geosyst.* **11**, (2010).
- Lowenstern, J. B., Evans, W. C., Bergfeld, D. & Hunt, A. G. Prodigious degassing of a billion years of accumulated radiogenic helium at Yellowstone. *Nature* **506**, 355–358 (2014).
- Sano, Y., Wakita, H. & Huang, C. Helium flux in a continental land area estimated from $^3\text{He}/^4\text{He}$ ratio in northern Taiwan. *Nature* **323**, 55–57 (1986).
- Lan, T. F. et al. Evaluating Earth degassing in subduction zones by measuring helium fluxes from the ocean floor. *Earth Planet. Sci. Lett.* **298**, 317–322 (2010).

44. Su, X. et al. Magma system and equilibrium depth of the Cenozoic basalts in the central North China craton. *Lithos* **446**, 107142 (2023).
45. Zhang, W., Du, J., Zhou, X. & Wang, F. Mantle volatiles in spring gases in the Basin and Range Province on the west of Beijing, China: Constraints from helium and carbon isotopes. *J. Volcanol. Geotherm. Res* **309**, 45–52 (2016).
46. Kaislaniemi, L. & van Hunen, J. Dynamics of lithospheric thinning and mantle melting by edge-driven convection: Application to Moroccan Atlas mountains. *Geochem. Geophys. Geosyst.* **15**, 3175–3189 (2014).
47. Zahirovic, S., Müller, R. D., Seton, M. & Flament, N. Tectonic speed limits from plate kinematic reconstructions. *Earth Planet. Sci. Lett.* **418**, 40–52 (2015).
48. Zhao, D., Yu, S. & Ohtani, E. East Asia: Seismotectonics, magmatism and mantle dynamics. *J. Asian Earth Sci.* **40**, 689–709 (2011).
49. Tao, K., Grand, S. P. & Niu, F. Seismic structure of the upper mantle beneath eastern Asia from full waveform seismic tomography. *Geochem. Geophys. Geosyst.* **19**, 2732–2763 (2018).
50. Choi, H. O., Choi, S. H., Lee, D. C. & Kang, H. C. Geochemical evolution of basaltic volcanism within the tertiary basins of southeastern Korea and the opening of the East Sea (Sea of Japan.). *J. Volcanol. Geotherm. Res.* **249**, 109–122 (2013).
51. Choi, S. H., Mukasa, S. B., Kwon, S. T. & Andronikov, A. V. Sr Nd, Pb and Hf isotopic compositions of late Cenozoic alkali basalts in South Korea: Evidence for mixing between the two dominant asthenospheric mantle domains beneath East Asia. *Chem. Geol.* **232**, 134–151 (2006).
52. Matsuda, J. et al. The $3\text{He}/4\text{He}$ ratio of the new internal He Standard of Japan (HESJ). *Geochem. J.* **36**, 191–195 (2002).
53. Craig, H., Clarke, W. B. & Beg, M. A. Excess 3He in deep water on the East Pacific Rise. *Earth Planet. Sci. Lett.* **26**, 125–132 (1975).
54. Craig, H., Lupton, J. E. & Horibe, Y. A mantle helium component in circum-Pacific volcanic gases: Hakone, the Marianas, and Mt. Lassen. *Terr. rare gases* **3**, 3–16 (1978).
55. Chang, S. J. & Baag, C. E. Moho depth and crustal VP/VS variation in Southern Korea from teleseismic receiver functions: Implication for tectonic affinity between the Korean Peninsula and China. *Bull. Seismol. Soc. Am.* **97**, 1621–1631 (2007).
56. Kim, Y. H., Lee, C. & Kim, S. S. Tectonics and volcanism in East Asia: Insights from geophysical observations. *J. Asian Earth Sci.* **113**, 842–856 (2015).
57. Lee, D. H., Lee, J. M., Cho, H. M. & Kang, T. S. 3D crustal velocity structure beneath the broadband seismic array in the Gyeongju area of Korea by receiver function analyses. *Tectonophysics* **689**, 89–106 (2016).
58. Andrews, J. N. & Lee, D. J. Inert gases in groundwater from the Bunter Sandstone of England as indicators of age and palaeoclimatic trends. *J. Hydrol.* **41**, 233–252 (1979).
59. Graham, D. W. Noble gas isotope geochemistry of mid-ocean ridge and ocean island basalts: Characterization of mantle source reservoirs. *Rev. Mineral. Geochem.* **47**, 247–317 (2002).
60. Rudnick, R. L. & Gao, S. Composition of the Continental Crust. in *Treatise on Geochemistry* vol. 3 1–64 (Pergamon, 2003).
61. Kulongoski, J. T., Hilton, D. R. & Izbicki, J. A. Source and movement of helium in the eastern Morongo groundwater Basin: The influence of regional tectonics on crustal and mantle helium fluxes. *Geochim. Cosmochim. Acta* **69**, 3857–3872 (2005).
62. Menzies, C. D. et al. The fluid budget of a continental plate boundary fault: Quantification from the Alpine Fault, New Zealand. *Earth Planet. Sci. Lett.* **445**, 125–135 (2016).
63. Jeong, C. H., Hur, H. S., Nagao, K. & Kim, K. H. Hydrochemical and isotopic characteristics, and origin of noble gas for low-temperature hot spring waters in the honam area. *Econ. Environ. Geol.* **40**, 635–649 (2007).
64. Kim, K. H., Jeong, Y. J., Jeong, C. H. & Keisuke, N. Hydrogeochemical, stable and noble gas isotopic studies of hot spring waters and cold groundwaters in the seokmodo hot spring area of the Ganghwa Province, South Korea. *Econ. Environ. Geol.* **41**, 15–32 (2008).
65. Park, J. et al. Hydrochemistry and noble gas geochemistry of geothermal waters in Chungcheong Province, South Korea. *Geochem. J.* **50**, 89–103 (2016).
66. Jeong, C. H. et al. Hydrochemistry and noble gas origin of hot spring waters of Icheon and Pocheon area in Korea. *J. Eng. Geol.* **19**, 529–541 (2009).

Acknowledgements

This study was sponsored by the National Research Foundation of Korea (NRF) grant funded by the Ministry of Science and ICT (2022R1A5A1085103 and 2020M1A5A1110629) and the Ministry of Trade, Industry and Energy, Korea (00426295-G03004262951-10054408). This work was also supported by the principal Research Fund of the Korea Institute of Geoscience and Mineral Resources. We are grateful to Myungok Jeong, Jong Gil Choi for their support on sampling.

Author contributions

H.K. and H.L. designed the study and wrote the manuscript together. J.-H.S., W.L., and J.H. contributed to sample acquisition. T.K. and N.T., Y.S. and T.F. jointly performed the interpretation of the analyzed results.

Competing interests

The authors declare no competing interests.

Additional information

Supplementary information The online version contains supplementary material available at <https://doi.org/10.1038/s43247-024-01592-4>.

Correspondence and requests for materials should be addressed to Hyunwoo Lee.

Peer review information *Communications Earth & Environment* thanks Richard Ernst and the other, anonymous, reviewer(s) for their contribution to the peer review of this work. Primary Handling Editors: Lucia Pappalardo and Carolina Ortiz Guerrero. A peer review file is available.

Reprints and permissions information is available at <http://www.nature.com/reprints>

Publisher's note Springer Nature remains neutral with regard to jurisdictional claims in published maps and institutional affiliations.

Open Access This article is licensed under a Creative Commons Attribution-NonCommercial-NoDerivatives 4.0 International License, which permits any non-commercial use, sharing, distribution and reproduction in any medium or format, as long as you give appropriate credit to the original author(s) and the source, provide a link to the Creative Commons licence, and indicate if you modified the licensed material. You do not have permission under this licence to share adapted material derived from this article or parts of it. The images or other third party material in this article are included in the article's Creative Commons licence, unless indicated otherwise in a credit line to the material. If material is not included in the article's Creative Commons licence and your intended use is not permitted by statutory regulation or exceeds the permitted use, you will need to obtain permission directly from the copyright holder. To view a copy of this licence, visit <http://creativecommons.org/licenses/by-nc-nd/4.0/>.

© The Author(s) 2024